Robotica: (2019) volume 37, pp. 1383–1400. © The Author(s), 2019. Published by Cambridge University Press. This is an Open Access article, distributed under the terms of the Creative Commons Attribution-NonCommercial-NoDerivatives licence (https://creativecommons.org/licenses/by-nc-nd/4.0/), which permits non-commercial re-use, distribution, and reproduction in any medium, provided the original work is unaltered and is properly cited. The written permission of Cambridge University Press must be obtained for commercial re-use or in order to create a derivative work.
doi:10.1017/S0263574719000018

Topology and Size–Shape Optimization of an Adaptive Compliant Gripper with High Mechanical Advantage for Grasping Irregular Objects

Chih-Hsing Liu*, Chen-Hua Chiu, Mao-Cheng Hsu, Yang Chen and Yen-Pin Chiang

Department of Mechanical Engineering, National Cheng Kung University, Tainan, Taiwan.
E-mails: zas988777@gmail.com, qwe.566@gmail.com, balrog705@gmail.com, slslpc1031@gmail.com

(Accepted January 1, 2019. First published online: February 1, 2019)

SUMMARY
This study presents an optimal design procedure including topology optimization and size–shape optimization methods to maximize mechanical advantage (which is defined as the ratio of output force to input force) of the synthesized compliant mechanism. The formulation of the topology optimization method to design compliant mechanisms with multiple output ports is presented. The topology-optimized result is used as the initial design domain for subsequent size–shape optimization process. The proposed optimal design procedure is used to synthesize an adaptive compliant gripper with high mechanical advantage. The proposed gripper is a monolithic two-finger design and is prototyped using silicon rubber. Experimental studies including mechanical advantage test, object grasping test, and payload test are carried out to evaluate the design. The results show that the proposed adaptive complaint gripper assembly can effectively grasp irregular objects up to 2.7 kg.

KEYWORDS: Topology optimization; Size–shape optimization; Mechanical advantage; Compliant mechanism; Compliant gripper.

1. Introduction

Compliant mechanisms are flexible members that can operate through elastic deformation. To synthesize compliant mechanisms, topology optimization is one major approach, which begins with an initial design domain with specific loading and boundary conditions. Generally, the first step of topology optimization is to discretize the analysis domain into finite elements, and different numerical algorithms can be used to identify the optimal layout of the material in the analysis domain. The algorithms of topology optimization have been widely investigated and developed during the past several decades.[1–5] The concept of traditional finite element-based topology optimization is to remove inefficient elements from a discretized domain iteratively until an optimal material layout is obtained. Traditionally, the element update scheme can be classified into two categories, hard-kill and soft-kill. The hard-kill scheme deletes unnecessary elements directly from the structure, whereas the soft-kill scheme reduces the pseudo densities (or elastic moduli) of inefficient elements to a small positive value to represent void elements. A material interpolation and penalization scheme[6–9] can also be used, which allows to vary the density of each element from a small value to one by a small increment. The more recent approaches such as the bidirectional evolutionary structural optimization (BESO) method[10–13] and sequential element rejection and admission (SERA) method[14,15] allow

* Corresponding author. E-mail: chliu@mail.ncku.edu.tw

https://doi.org/10.1017/S0263574719000018 Published online by Cambridge University Press

elements to be removed and added simultaneously within each iteration according to the variations of sensitivity numbers. A prespecified value for volume fraction, which is defined as the calculated volume divided by the full volume of the analysis domain, is used as the constraint in the topology optimization process. In topology synthesis of compliant mechanisms,[13–22] the usage of numerical springs located at the desired input and output ports of the analyzed compliant mechanism is one general method to specify the input and output locations. Due to the presence of the input and output springs in the analysis domain, the calculated nodal displacements are extremely small; thus, linear elastic finite element formulation is valid in the topology optimization process. The objective function of traditional topology synthesis of continuum structures is to minimize strain energy of the analysis domain, which is equivalent to maximizing the structural stiffness while satisfying the prespecified volume fraction constraint. For the synthesis of compliant mechanisms, the objective functions are used to maximize mutual potential energy[14–18] and geometric advantage (which is defined as the ratio of output displacement to input displacement).[17–19,21,22] A non-dimensional objective function based on the ratio of mutual potential energy and the sum of input and output strain energy is also proposed,[23] which can consider both geometric advantage and mechanical advantage of the synthesized compliant mechanism by a user-specified advantage control parameter; increasing the advantage control parameter would increase the geometric advantage and decrease the mechanical advantage of the mechanism (and vice versa).[23] Mechanical advantage is defined as the ratio of output force to input force. The product of geometric advantage and mechanical advantage of a mechanism is referred to as the mechanical efficiency.[16]

Various topology optimization methods are used to synthesize compliant grippers.[15,16,22,24,25] A dexterous robotic gripper is expected to perform grasping tasks for handling of objects with size and shape variations, which usually requires several actuators to execute the planning motion. Since the control strategy and mechanism become complex for a design with increasing actuators, the usage of underactuated mechanisms becomes a good practical option.[26] In contrast, compliant mechanisms usually offer a unique feature (compared with rigid mechanisms) that allows compliant members to be adaptive in a limited range during operation, and can also prevent possible damage to the objects being handled. The materials with elastic moduli in the order of $10^4 \sim 10^9$ are considered soft materials,[27] which can be used to form soft mechanisms and robots. In contrast to rigid mechanisms and robots that have moduli in the order of $10^9 \sim 10^{12}$, soft robots such as soft hands,[28–30] soft grippers,[24,31,32] or soft manipulators[33,34] usually have the ability to gently grip and maneuver vulnerable objects. Soft graspers can be used in the handling of delicate food products[35–38] as most natural food products are variable in shape and easily bruised.[35] Some special gripper designs for harvesting horticulture products such as tomato[39,40] and strawberry[41] are also proposed. Some control schemes such as constrained linear quadratic optimization method[42,43] and a feedforward controller based on both flexible and rigid body modes[44] can be used for vibration suppression and robust tracking of flexible systems. One possible disadvantage in the usage of soft compliant mechanisms than rigid mechanisms is that the mechanical advantage of a compliant member is usually lower than that of rigid mechanisms with the same dimensions. In other words, the output force of a compliant mechanism is usually lower than its rigid counterpart at the same given input force.

Motivated by the need to minimize the problem of compliant mechanisms that usually generate lower output force, this paper aims to develop an optimal design procedure including topology and size–shape optimization methods to maximize mechanical advantage (or output force) of the synthesized compliant mechanism. In addition, the proposed procedure is used to design an adaptive compliant gripper with high mechanical advantage and multiple desired output ports. The remaining part of this paper offers the following content: the formulations of the topology and size–shape optimization methods are introduced in Section 2. The result of the optimal design of the proposed adaptive compliant gripper is provided in Section 3. The proposed gripper is prototyped using silicon rubber, and experimental tests (including mechanical advantage test, object grasping test, and payload test) are carried out to evaluate the design. The experimental results are summarized in Section 4. Finally, the conclusion is made in Section 5.

2. Optimal Design Methods

The optimal design methods used in this study consist of topology optimization method and size–shape optimization method. The topology optimization method is used to synthesize the optimal layout of the analyzed compliant mechanism. Then the identified optimal topology is used as the

https://doi.org/10.1017/S0263574719000018 Published online by Cambridge University Press

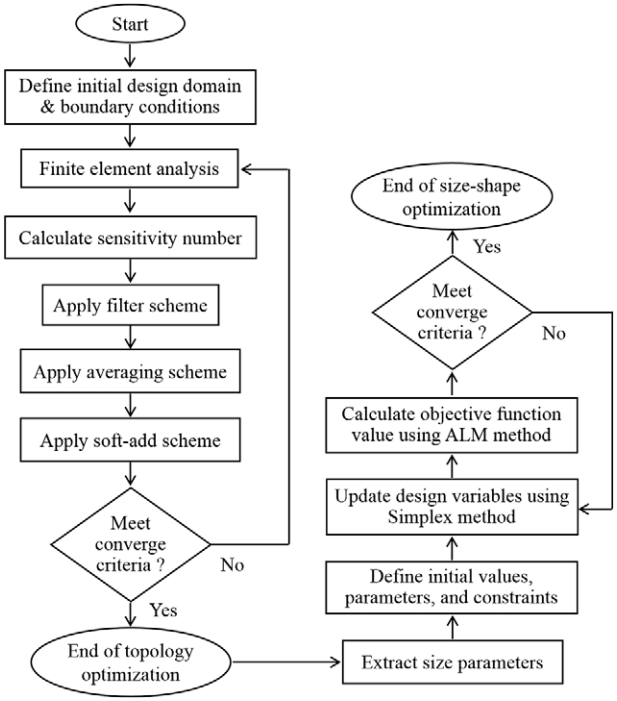

Fig. 1. Flowchart of the topology optimization and size–shape optimization procedure.

initial design domain for size–shape optimization. The flowchart of the proposed topology and size–shape optimization procedure is given in Fig. 1. The optimization procedure starts with an initial design domain with prespecified boundary conditions. The finite element method is used to solve the force equilibrium problem. The sensitivity number of each element can be computed by calculating the gradient of the objective function with respect to the design variable. A filter scheme is used to avoid possible mesh dependency and checkerboard pattern problems[45–48]; then an averaging scheme is used to increase the numerical stability of the topology optimization process. A soft-add scheme[22] is used to update sensitivity number and pseudo density of each element. Unlike the traditional hard-kill and soft-kill methods, a special characteristic of the soft-add scheme is that the elements are equivalent to be numerically added into the analysis domain. After an optimal topology of the analyzed compliant mechanism is obtained, the optimal layout of the structure from the result of topology optimization is served as the initial design domain for size–shape optimization. The size–shape optimization method used in this study is a mixed method combining both Augmented Lagrange Multiplier (ALM) method[49] and Simplex method.[49] The design variables are updated using Simplex method, and the objective function value is calculated using ALM method. On completing the size–shape optimization procedure, the optimal design can be obtained. The detailed formulations of the proposed topology and size–shape optimization methods are provided in the following paragraphs. The numerical computation is performed in Matlab R2015 environment.

2.1. Topology optimization method for the design of compliant mechanisms with multiple output ports

The proposed topology optimization method discussed in this section is used to synthesize a monolithic compliant gripper for grasping irregular objects. The objective function of the proposed method is capable of maximizing either mechanical advantage or geometric advantage of the analyzed compliant mechanism with one input and multiple target output ports. The proposed approach is used to design a two-finger compliant gripper. Two target output ports are defined for each finger in this study. To minimize the problem of compliant mechanisms that usually generate lower output force, the objective function of the proposed gripper is set to maximize its mechanical advantage. The working principle of the two-finger compliant gripper is illustrated in Fig. 2(a). The half-symmetric compliant gripper is actuated by an input displacement provided at the input port, and can generate grasping motion through elastic deformation of the gripper. The desired output port #1 is at the fingertip of the gripper, and the desired output port #2 is at the midpoint of the finger. The two-output port design

https://doi.org/10.1017/S0263574719000018 Published online by Cambridge University Press

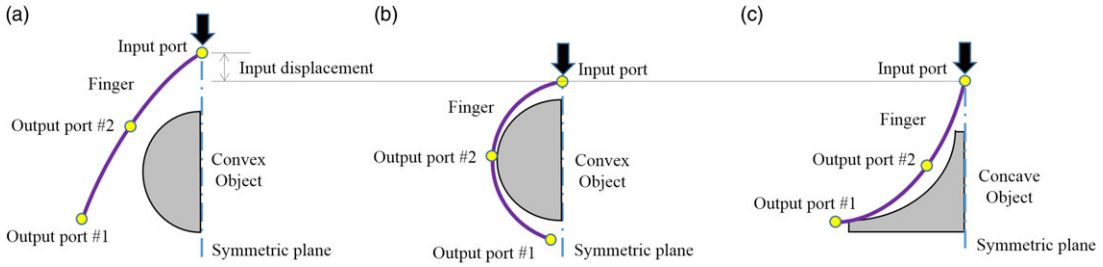

Fig. 2. Working principle and grasping strategy of the compliant gripper (half-symmetric model): (a) working principle of the two-finger compliant gripper, (b) grasping strategy for a convex object, and (c) grasping strategy for a concave object.

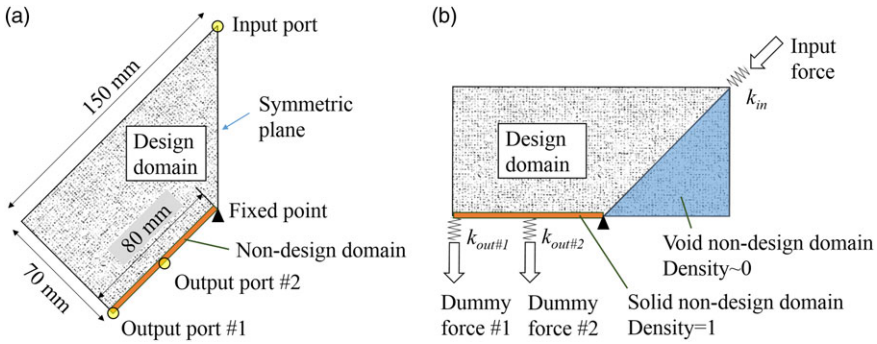

Fig. 3. Design domain and boundary conditions for topology optimization of the compliant gripper (half-symmetric model): (a) design domain and (b) analysis domain.

is corresponding to the grasping strategy of the gripper, which is illustrated in Fig. 2(b) and (c). For the scheme of grasping a convex object as illustrated in Fig. 2(b), the displacement output at the desired output port #1 will help the finger to enclose the convex object. In contrast, for the scheme of grasping a concave object as illustrated in Fig. 2(c), the displacement output at the desired output port #2 will help the finger to accommodate the geometry of the concave object. The two-output port design will help the finger to grasp objects with shape variation.

The design domain of topology optimization of the compliant gripper discussed in Fig. 2 is shown in Fig. 3(a). As the desired gripper in this study is a two-finger design, a half-symmetric model is used in the topology optimization process. The design domain in Fig. 3(a) consists of one input port and two target output ports (for each finger). The expected contact region of the finger is defined as the solid non-design domain, which is also the length of the finger. The desired output port #1 is at the fingertip, and the desired output port #2 is at the midpoint of the expected contact region. Figure 3(b) provides the analysis model for topology optimization, which is meshed by square finite elements. Numerical springs (k_{in} and k_{out}) are added at input and output ports in the optimization model. The input force is specified at the input port, and dummy forces are specified at both output ports as shown in Fig. 3(b). According to the dummy load method,[14,15,25] each dummy load is a unit force applied at the desired output port in the direction of the desired displacement. The design variable in this study is the pseudo density of each element, which can be varied from 0 to 1 by a small increment. The pseudo densities of the elements at the expected contact region (solid non-design domain) are defined as 1 throughout the optimization process, whereas the elements in the right triangular region (void non-design domain) in Fig. 3(b) are defined as 0 to represent the void elements. In practice, the pseudo density of 0 is replaced by a small positive value $x_{\min}$ to avoid singularity.

The proposed objective function of topology synthesis of compliant mechanisms with one input and n target output ports is formulated as the following strain energy-based function:

$$c = \frac{\sum_{i=1}^{n} \zeta_i S_{\text{mut},i}}{2\eta S_{\text{in}} + 2\,(1-\eta)\left[\sum_{i=1}^{n} \zeta_i S_{\text{out},i}\right]}, \quad \text{where} \sum_{i=1}^{n} \zeta_i = 1 \tag{1}$$

where c is the objective function to be maximized; η is the advantage control parameter; decreasing η would increase the mechanical advantage and decrease the geometric advantage of the mechanism;[23]

https://doi.org/10.1017/S0263574719000018 Published online by Cambridge University Press

ζ is the output control parameter (weighting factor), which controls the output ratio of each output port; S_{in}, S_{out}, and S_{mut} are input strain energy, output strain energy, and mutual potential energy, respectively; their formulations are:

$$S_{\text{in}} = \frac{1}{2}\int_{\Omega} \sigma\ (u_{\text{in}})\ \varepsilon\ (u_{\text{in}})\ dV \tag{2}$$

$$S_{\text{out}} = \frac{1}{2}\int_{\Omega} \sigma\ (u_{\text{out}})\ \varepsilon\ (u_{\text{out}})\ dV \tag{3}$$

$$S_{\text{mut}} = \int_{\Omega} \sigma\ (u_{\text{out}})\ \varepsilon\ (u_{\text{in}})\ dV \tag{4}$$

The energy-based objective function given in Eq. (1) is motivated by the objective function proposed by Krishnakumar and Suresh,[23] which can be used to generate compliant mechanisms with different geometric and mechanical advantages by varying a single control parameter (η). In addition to the original objective function, a new weighting factor (ζ) is proposed in this study to account for the optimization problem with multiple output ports via the weighted sum method. To design a compliant gripper with two target output ports (for each finger) as specified in Fig. 3, the objective function in Eq. (1) can be reformulated as:

$$\text{Maximize: } c = \frac{\zeta_1 S_{\text{mut},1} + \zeta_2 S_{\text{mut},2}}{2\eta S_{\text{in}} + 2\,(1-\eta)\left[\zeta_1 S_{\text{out},1} + \zeta_2 S_{\text{out},2}\right]} \tag{5}$$

$$\text{Subject to: } \mathbf{K}\mathbf{U}_1 = \mathbf{F}_1;\ \ \mathbf{K}\mathbf{U}_2 = \mathbf{F}_2\ ;\ \ \mathbf{K}\mathbf{U}_3 = \mathbf{F}_3$$

$$\sum_{i=1}^{N} x_i V_e = V^*;\ \ 0 < x_{\min} \le x_i \le 1$$

$$0 < \eta < 1\ ;\ \ \zeta_1 + \zeta_2 = 1 \tag{6}$$

where $\mathbf{F}_1$ is the global force vector while only the input force is acting at the input port; $\mathbf{F}_2$ is the global force vector while only the unit dummy force #1 is acting at the output port #1; $\mathbf{F}_3$ is the global force vector while only the unit dummy force #2 is acting at the output port #2; $\mathbf{K}$ is the global stiffness matrix; $\mathbf{U}_1$, $\mathbf{U}_2$, and $\mathbf{U}_3$ are the displacement vectors corresponding to the force vectors $\mathbf{F}_1$, $\mathbf{F}_2$, and $\mathbf{F}_3$, respectively; V^* is the target volume; x_i is the pseudo density of the ith element; $x_{\min}$ is a very small positive value used to represent void elements numerically; V_e is the volume of an element; N is the total number of elements in the analysis domain; S_{in} is the input strain energy; $S_{\text{out},1}$ and $S_{\text{out},2}$ are output strain energy; $S_{\text{mut},1}$ and $S_{\text{mut},2}$ are mutual potential energy; their formulations are:

$$S_{\text{in}} = \frac{1}{2}\mathbf{U}_1^T\mathbf{K}\mathbf{U}_1;\quad S_{\text{out},1} = \frac{1}{2}\mathbf{U}_2^T\mathbf{K}\mathbf{U}_2;\quad S_{\text{out},2} = \frac{1}{2}\mathbf{U}_3^T\mathbf{K}\mathbf{U}_3;$$

$$S_{\text{mut},1} = \mathbf{U}_2^T\mathbf{K}\mathbf{U}_1;\quad S_{\text{mut},2} = \mathbf{U}_3^T\mathbf{K}\mathbf{U}_1 \tag{7}$$

The global stiffness matrix $\mathbf{K}$ is formulated as:

$$\mathbf{K} = \mathbf{K}_s + \sum_e x_i^p \mathbf{K}_e \tag{8}$$

where $\mathbf{K}_s$ is the stiffness matrix of the numerical springs placed at the desired input and output ports of the analyzed compliant mechanism; $\mathbf{K}_e$ is the element stiffness matrix; p is a penalty factor.

The elemental sensitivity number can be obtained by calculating the gradient of the objective function with respect to the design variable:

$$\alpha_{e,i} = \frac{\partial c}{\partial x_i} \tag{9}$$

The filter scheme discussed in the BESO method[12] is used in this study to avoid mesh dependency and checkerboard pattern problems in topology optimization. The first step in the filter scheme is to calculate the nodal sensitivity number $\alpha_{n,j}$:

$$\alpha_{n,j} = \frac{\sum_{i=1}^{n_e} \alpha_{e,i}}{n_e} \tag{10}$$

https://doi.org/10.1017/S0263574719000018 Published online by Cambridge University Press

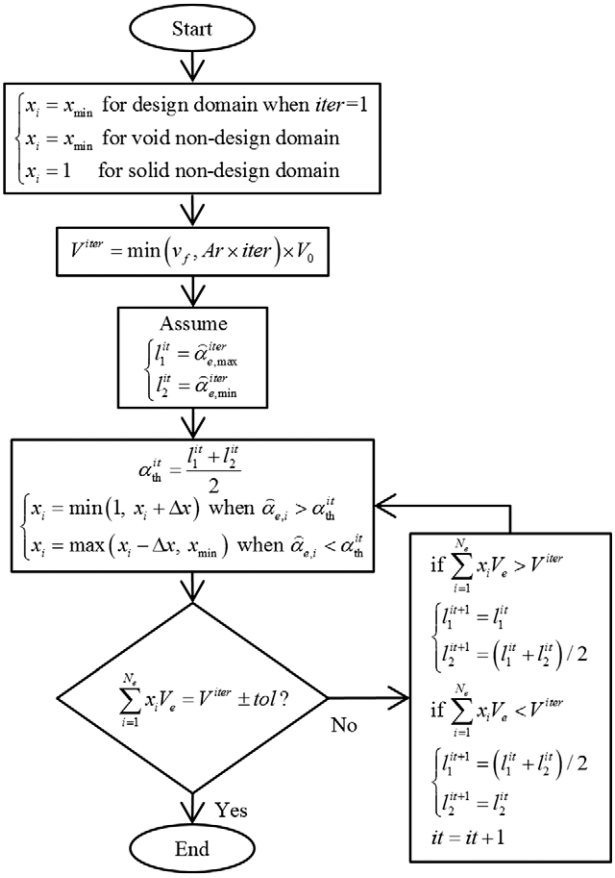

Fig. 4. Update scheme.

where $\alpha_{e,i}$ is the elemental sensitivity number obtained by Eq. (9); i and j denote the element number and node number, respectively; n_e is the total number of elements connected to the jth node.

The filtered elemental sensitivity number can be defined as:

$$\tilde{\alpha}_{e,i} = \frac{\sum_{j=1}^{n_r} w_{ij} \times \alpha_{n,j}}{\sum_{j=1}^{n_r} w_{ij}} \tag{11}$$

$$w_{ij} = \max(0, r - r_{ij}) \tag{12}$$

where $\alpha_{n,j}$ is the nodal sensitivity number; w_{ij} is a weight factor; r is the filter radius about the center of the ith element; r_{ij} is the distance between the jth node and the center of the ith element; n_r denotes the total number of nodes within the circle of the filter radius.

The averaging scheme[12] of the filtered elemental sensitivity numbers for every two successive iterations is applied in this study to stabilize the evolutionary process:

$$\tilde{\alpha}_{e,i}^{iter} = \frac{\tilde{\alpha}_{e,i}^{iter} + \tilde{\alpha}_{e,i}^{iter-1}}{2}; \quad iter = 2, 3, \ldots \tag{13}$$

where $iter$ is iteration number; $\tilde{\alpha}_{e,i}^{iter}$ is the filtered elemental sensitivity number at specific iteration. By using this approach, the updated sensitivity numbers include all previous historical sensitivity information.

After filtering and averaging schemes are performed, a soft-add update scheme[22] as given in Fig. 4 is used to update the pseudo densities, sensitivity numbers, and the volume constraint. In the soft-add scheme, the pseudo densities of all elements in the design domain are initially defined as $x_{\min}$, and the calculated volume of each iteration, V^{iter}, is defined as:

$$V^{iter} = \min(v_f, Ar \times iter) \times V_0 \tag{14}$$

https://doi.org/10.1017/S0263574719000018 Published online by Cambridge University Press

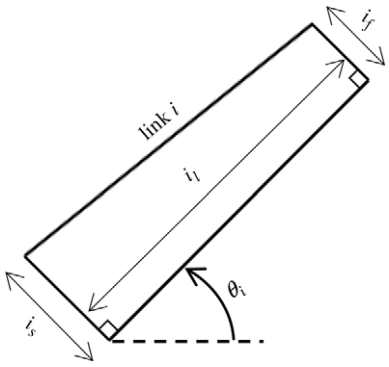

Fig. 5. Equivalent trapezoidal linkage.

where v_f is the predefined volume fraction constraint that represents the target volume of the optimized compliant mechanism divided by the total volume of the global analysis domain; Ar is a predefined variation value; *iter* is iteration number; V_0 is the full volume when all elements exist in the analysis domain. The calculated volume of each iteration is initially determined by multiplying the iteration number, the variation value Ar, and the total volume V_0. The calculated volume V^{iter} is linearly increased with the iteration number until the volume fraction constraint v_f is reached, then the calculated volume remains constant ($v_f \times V_0$) until the numerical computation is converged.

A threshold value α_{th}^{it} of the sensitivity number for each local iteration (*it*) is defined as the average of the minimum and maximum elemental sensitivity numbers in a global iteration (*iter*). If the filtered elemental sensitivity number of the *i*th element is larger than the threshold value, the pseudo density of the *i*th element (x_i) is increased by one increment Δx in the local iteration (*it*); otherwise, the pseudo density is decreased by one increment in the local iteration if the filtered elemental sensitivity number of an element is smaller than the threshold value. The pseudo density of each element is initially assigned with the same value as $x_{\min}$, which is a very small positive value. In addition, the pseudo density of each element can be varied (increased or decreased) from x_{min} to one with a small increment Δx during the iterative process in this approach.

The volume of each global iteration can be calculated by summation of the pseudo densities times the element volumes of the analysis domain:

$$V^{iter} = \sum_{i=1}^{N_e} x_i \mathrm{V}_e \tag{15}$$

where N_e is the total number of elements in the analysis domain; x_i is the pseudo density of the *i*th element; V_e is the volume of an element. If the obtained value in Eq. (15) is different from the previously determined volume in Eq. (14), a new threshold value can be calculated based on the update scheme in Fig. 4.

The following convergence criterion, which calculates the difference in the sum of the objective function value for each successive five iterations, is used to check for the termination.

$$\left| \frac{\sum_{n=iter-9}^{iter-5} c_n - \sum_{n=iter-4}^{iter} c_n}{\sum_{n=iter-4}^{iter} c_n} \right| \leq err \,,\; iter \geq 10 \tag{16}$$

where c is the objective function as given in Eq. (5); n is number; *err* is an allowable tolerance.

2.2. Size–shape optimization method

The optimal design of the compliant mechanism from topology optimization is used as the initial design domain for the size–shape optimization process in this study. The flowchart of the proposed size–shape optimization procedure is given in Fig. 1. The size parameters are extracted from the optimal topology. A proposed equivalent trapezoidal linkage model is used in this study. In this approach, the right-angled trapezoids are deployed to the optimized topology to approximate the identified layout from topology optimization. Each trapezoidal link has one angle and three size parameters as illustrated in Fig. 5, which are the angle of the link and height and two bases of the

https://doi.org/10.1017/S0263574719000018 Published online by Cambridge University Press

right-angled trapezoid. For example, in Fig. 5, the angle of link i is denoted as θ_i (which is the angle between x-axis and the right-angled leg of the trapezoid); the length of link i is denoted as i_l (which is the height of the right-angled trapezoid); the two bases of the right trapezoid are denoted as i_f and i_s. The initial values of these parameters are identified from the comparison between the equivalent trapezoidal linkage model and the identified layout from topology optimization.

A mixed method combining Augmented Lagrange Multiplier (ALM) method,[49] Simplex method,[49] and nonlinear finite element analysis (FEA) using commercial software is used in the size–shape optimization process. As the flowchart given in Fig. 1, after the size parameters are extracted using the previously described equivalent trapezoidal linkage model, the Simplex method is used to update the design variables. The objective function value is calculated using the ALM method. The augmented Lagrangian function, $A(\boldsymbol{X}, \lambda, \gamma_p)$, is defined as the combination of the objective function (which is mechanical advantage in this study), Lagrange multipliers, and penalty parameter. The mechanical advantage of the half-symmetric gripper model is obtained using the FEA software, ANSYS, to solve the nonlinear problem. A tolerance value is predefined for convergence evaluation. If the difference of the highest and lowest augmented Lagrangian function values is larger than the tolerance value (which is 0.0001 in this study), the Simplex method is used to update design variables, which can calculate a centroid value for the reflection operation.[49] Then the Lagrange multiplier and penalty parameter can be further updated to start the next round of iteration until convergence. The numerical computation is implemented in Matlab R2015 environment, while ANSYS is executed in batch mode to perform the geometrically nonlinear FEA. The objective function and constraints of the size–shape optimization problem are formulated as:

$$\text{Maximize: } A\left(\boldsymbol{X}, \lambda, \gamma_p\right) = f(\boldsymbol{X}) + \sum_{j=1}^{m}\left[\lambda_j \psi_j + \gamma_p \psi_j^2\right]$$

$$\text{where } \psi_j = \max\left[g_j(\boldsymbol{X}), \frac{-\lambda_j}{2\gamma_p}\right] \tag{17}$$

$$\text{Subject to: } g_j(\boldsymbol{X}),\ j = 1 \text{ to } m \tag{18}$$

where $A(\boldsymbol{X}, \lambda, \gamma_p)$ is the augmented Lagrangian function; $f(\boldsymbol{X})$ is mechanical advantage in this study (which can also be replaced by geometric advantage if the objective of optimization is to maximize geometric advantage instead of mechanical advantage); λ_j are Lagrange multipliers; γ_p is penalty parameter; $g_j(\boldsymbol{X})$ are inequality constraints; m is the total number of constraints. The objective function given in Eq. (17) is the combination of mechanical advantage, Lagrange multipliers, and constraints, which is equivalent to maximizing the mechanical advantage of the analyzed mechanism.

3. Optimal Design of a Compliant Gripper to Maximize Mechanical Advantage

The optimal design methods (including topology optimization and size–shape optimization) discussed in the previous section are used to synthesize a compliant gripper with the objective to maximize its mechanical advantage. The design domain of the compliant gripper for topology optimization is given in Fig. 3. The output control parameters (ζ_1 and ζ_2) define the weighting factors of the two target output ports (as given in Fig. 3); the ratios of both output ports are defined as 50% in this study. To maximize the mechanical advantage of the synthesized compliant gripper in topology optimization process, the advantage control parameter (η) is defined as 0.01 according to a finding from Krishnakumar and Suresh[23] that decreasing η would increase the mechanical advantage of the synthesized mechanism. The numerical parameters used in topology optimization of the compliant gripper are summarized in Table I. The analysis domain in Fig. 3(b) consists of three regions, which are design domain, void non-design domain (density = $x_{\min}$), and solid non-design domain (density = 1); the analysis domain is discretized by 75 × 35 linear square plane stress elements.

The numerical computation of the topology optimization process is converged after 193 iterations. Figure 6 shows the iterative results for the values of objective function and volume fraction. The left y-axis of Fig. 6 is the objective function value calculated using Eq. (5), whereas the right y-axis is the calculated volume fraction (Eq. (15) divided by full volume). Both objective function and volume fraction values are unitless. It is to be noticed that the objective function value can be maximized iteratively during the topology optimization process. According to the soft-add scheme discussed in a previous section, the volume fraction value is linearly increased with the iterations until the target volume (which is 20% of the analysis domain) is reached, then the calculated volume remains

https://doi.org/10.1017/S0263574719000018 Published online by Cambridge University Press

Table I. Parameters of topology optimization.

Parameter	Definition	Value
η	Advantage control parameter	0.01
ζ_1	Weighting factor for output port #1	0.5
ζ_2	Weighting factor for output port #2	0.5
v_f	Volume fraction	0.2
Ar	Variation value	0.01
$x_{\min}$	Minimum pseudo density	0.001
Δx	Pseudo density increment	0.01
r	Filter radius	3.5
p	Penalty parameter	3
err	Allowable tolerance in convergence criterion	0.001
tol	Allowable tolerance in update scheme	10^{-5}
k	Numerical spring stiffness	10^5 N/m
F	Input force	10^6 N
E	Elastic modulus	21.6 MPa
ν	Poisson's ratio	0.3

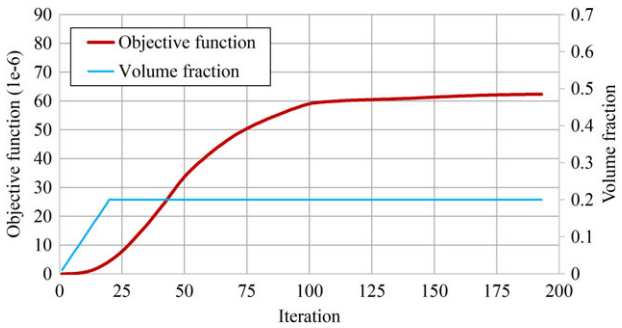

Fig. 6. Iterative results of objective function and volume fraction values.

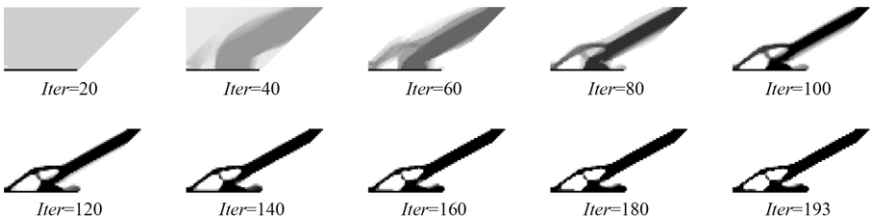

Fig. 7. Topology optimization of the complaint gripper (half-symmetric model): iterative results at some specific iterations.

constant until convergence. The topology optimization results at some specific iterations are given in Fig. 7, which is a half-symmetric model for the proposed complaint gripper. The white region in Fig. 7 denotes elements with pseudo densities equal to $x_{\min}$, whereas the dark region denotes elements with pseudo densities equal to 1. Gray region denotes elements with pseudo densities between $x_{\min}$ and 1. The $iter = 193$ result in Fig. 7 is the converged result of the topology optimization process. In addition, it is to be noticed that the iterative results of the optimal layout do not change significantly after 120 iterations.

The converged topology-optimized result given in Fig. 7 is used to generate the CAD model as shown in Fig. 8(a), whereas Fig. 8(b) shows its equivalent linkage model for size–shape optimization. Figure 8(c) shows the analysis condition of the finite element model for size–shape optimization. The detailed parameters in the equivalent linkage model as shown in Fig. 8(b) are given in the trapezoidal linkage model as shown in Fig. 9, where all design parameters for the size–shape optimization process are summarized in Table II. The thickness of each trapezoidal link in this study is defined as 10 mm. Figure 8(b) is a simplified representative model of Fig. 9. As shown in Fig. 9, the right-angled trapezoids are deployed to the topology model given in Fig. 8(a) to approximate the identified layout

https://doi.org/10.1017/S0263574719000018 Published online by Cambridge University Press

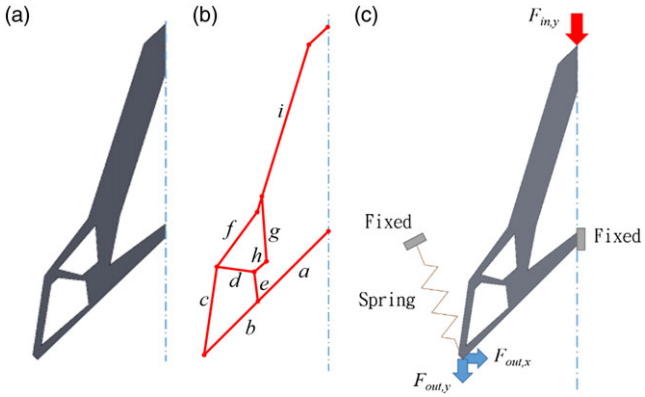

Fig. 8. Size–shape optimization model (half-symmetric model): (a) CAD model based on the topology-optimized result, (b) simplified equivalent linkage model for size–shape optimization, and (c) finite element analysis model for size–shape optimization.

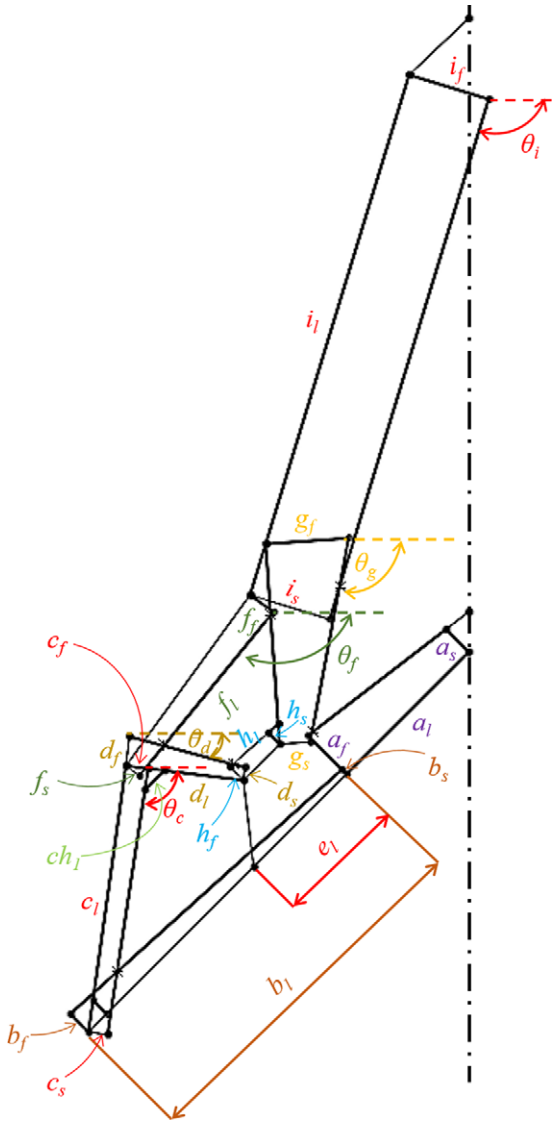

Fig. 9. Parameters of the trapezoidal linkage model for size–shape optimization.

https://doi.org/10.1017/S0263574719000018 Published online by Cambridge University Press

Table II. Parameters of size–shape optimization.

Design variable	Definition	Initial value	Optimal value	Variation %
a_l	Length of trapezoidal link *a*	27.0	27.32	1.2
a_f	Base #1 of trapezoidal link *a*	8.5	8.77	3.2
a_s	Base #2 of trapezoidal link *a*	5.0	2.99	**−40.2**
b_l	Length of trapezoidal link *b*	57.0	57.29	0.5
b_f	Base #1 of trapezoidal link *b*	4.0	4.30	7.5
b_s	Base #2 of trapezoidal link *b*	1.0	2.00	**100.0**
c_l	Length of trapezoidal link *c*	42.0	42.34	0.8
c_f	Base #1 of trapezoidal link *c*	3.5	3.82	9.1
c_s	Base #2 width of trapezoidal link *c*	3.0	3.33	**11.0**
θ_c	Angle of trapezoidal link *c*	−98.0	−97.89	−0.1
d_l	Length of trapezoidal link *d*	18.5	18.85	1.9
d_f	Base #1 of trapezoidal link *d*	4.6	4.94	7.4
d_s	Base #2 of trapezoidal link *d*	2.0	2.34	**17.0**
θ_d	Angle of trapezoidal link *d*	−7.0	−6.68	−4.6
e_l	Length of trapezoidal link *e*	20.5	20.84	1.7
f_l	Length of trapezoidal link *f*	33.0	33.34	1.0
f_f	Base #1 of trapezoidal link *f*	4.5	4.83	7.3
f_s	Base #2 of trapezoidal link *f*	2.6	2.93	**12.7**
θ_f	Angle of trapezoidal link *f*	−126.0	−125.66	−0.3
g_f	Base #1 of trapezoidal link *g*	13.0	13.33	2.5
g_s	Base #2 of trapezoidal link *g*	4.8	5.13	6.9
θ_g	Angle of trapezoidal link *g*	−86.0	−85.66	−0.4
h_l	Length of trapezoidal link *h*	8.0	8.35	4.4
h_f	Base #1 of trapezoidal link *h*	3.0	3.34	**11.3**
h_s	Base #2 of trapezoidal link *h*	2.5	2.84	**13.6**
i_l	Length of trapezoidal link *i*	85.0	85.34	0.4
i_f	Base #1 of trapezoidal link *i*	13.0	13.19	1.5
i_s	Base #2 of trapezoidal link *i*	13.0	13.26	2.0
θ_i	Angle of trapezoidal link *i*	−107.0	−106.68	−0.3
ch_1	Chamfer distance: links *c* and *d*	2.0	2.34	**17.0**
	Mechanical advantage	0.2687	0.2930	**9.0**

from topology optimization. The initial values of these parameters summarized in Table II are identified from comparison between the trapezoidal linkage model and the identified layout from topology optimization. As illustrated in Fig. 5, each trapezoidal link has one angle and three size parameters until the existence of other design constraints. For example, links *a* and *b* are the contact surface of the gripper, and θ_a and θ_b are predefined as the same constant value; thus θ_a and θ_b are not considered as design variables in the optimization process.

In the size–shape optimization process, geometrically nonlinear FEA (using the commercial software, ANSYS) is performed to calculate the mechanical advantage at the condition when the input displacement is 15 mm. Plane stress elements are used to mesh the size–shape optimization model as given in Fig. 8(c). The edge size of each element is defined as 1 mm. The mechanical advantage is obtained by calculating the ratio between the input force and vector sum output force as denoted in Fig. 8(c). A spring element connected to the fingertip is defined in order to measure the output force. The thickness of the gripper is 10 mm. The constraints of the size–shape optimization problem include: maximum allowable equivalent stress is 7 MPa (which is the yield strength of the material), and all size dimensions of the gripper should not be less than 2 mm (which is the minimum allowable dimension for the gripper to be manufactured by water jet cutting). The initial value and maximum value of the penalty parameter γ_p in ALM method are defined as 1 and 64, respectively.

The size–shape optimization process discussed in the previous section is used to identify the optimal design parameters of the compliant gripper. The size–shape optimization procedure is performed in Matlab environment. ANSYS is executed in batch mode to perform the geometrically nonlinear FEA via the input code in ANSYS parametric design language (APDL) compiled from Matlab. The ALM-Simplex algorithms and ANSYS are executed iteratively until convergence. The iterative process is converged after 62 iterations. The initial values, final values, and variations of all parameters

https://doi.org/10.1017/S0263574719000018 Published online by Cambridge University Press

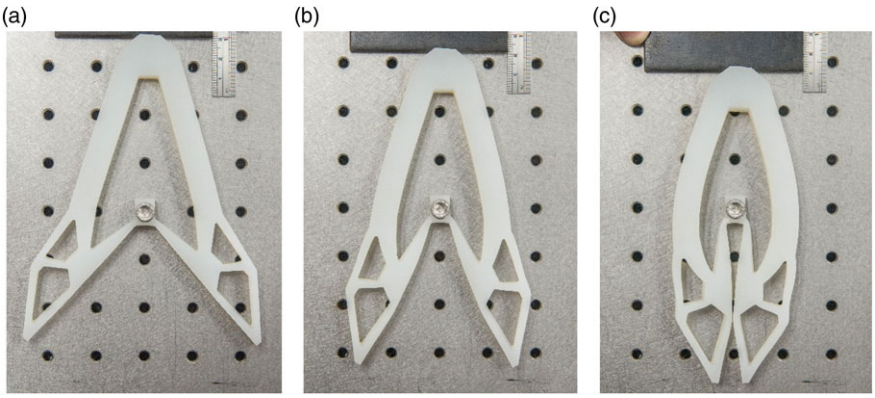

Fig. 10. Prototype of the compliant gripper: (a) no input displacement, (b) input displacement = 10 mm, and (c) input displacement = 20 mm.

are summarized in Table II. It is to be noticed that there are eight variables with more than 10% variation as summarized in Table II. Since the initial values of the size–shape optimization process are already topology-optimized, the variations of many design variables given in Table II are not significantly changed after size–shape optimization. The value of mechanical advantage is increased from 0.2687 to 0.2930 after the size–shape optimization process, which increases 9% compared with the original topology optimization design as shown in Fig. 8(a). The base #2 of trapezoidal link b (b_s) is the parameter with largest variation (100%, from 1 to 2 mm) after optimization, which is caused by the predefined minimum size constraint (as 2 mm is the minimum allowable dimension for the gripper to be manufactured by water jet cutting).

4. Prototype and Experimental Tests

The optimal design (as summarized in Table II) of the compliant gripper after topology optimization and size–shape optimization process is prototyped using water jet cutting (from a 10-mm-thick silicon rubber sheet). The prototype is shown in Fig. 10, which also shows the deformed shapes of the gripper when displacement input equals 10 and 20 mm. It is to be observed that the compliant gripper can be actuated by the displacement input specified at the input port. Figure 11 shows the input–output relationships of the compliant gripper at free movement condition (as illustrated in Fig. 10). The input displacement versus output displacement relations for output port #1 and port #2 (as defined in Fig. 3) of the gripper are given in Fig. 11(a); in this experiment, the gripper is placed on a grid paper and fixed at its fixed port. Both the input displacement at input port and the resultant output displacements at output port #1 and port #2 are measured by calculating the number of grids. The average geometric advantages of output port #1 and output port #2 are 2.6 and 1.5, respectively. Figure 11(b) shows the input displacement versus input force relationship for the gripper; in this experiment, a force sensor (Lutron FG-6005SD as shown in Fig. 12) is placed at the input port to measure the required input force to generate specific displacement input for the compliant gripper at free movement condition. Figure 11(b) shows that the input force required to generate 30 mm displacement input at input port for the compliant finger is 23 N.

The experimental setup for mechanical advantage test is given in Fig. 12. In the experiment, one single-axis force gauge (Lutron FG-6005SD) is placed at the input port to measure the input force, and a three-axis force sensor (OptoForce OMD-20-SE-40N) is placed at the target contact location (20 mm from the fingertip) to measure the output force at the fingertip (output port #1) at different input displacement conditions. The three-axis force sensor is then moved to the target contact location of output port #2 to measure the output force at the middle of the grip surface. The measurement results from the mechanical advantage test at different input displacement conditions are given in Fig. 13. Figure 13(a) shows the input and output force measurement results for one finger (a half gripper). The mechanical advantages for output port #1 and port #2 at different input displacement conditions are given in Fig. 13(b). It is to be noticed that the values of mechanical advantages are different at different input displacement conditions and different output ports. The 15 mm input displacement case for output port #1 measurement is the analysis condition in the previous size–shape optimization stage. Comparing the predicted optimal value (mechanical advantage = 0.293) as

https://doi.org/10.1017/S0263574719000018 Published online by Cambridge University Press

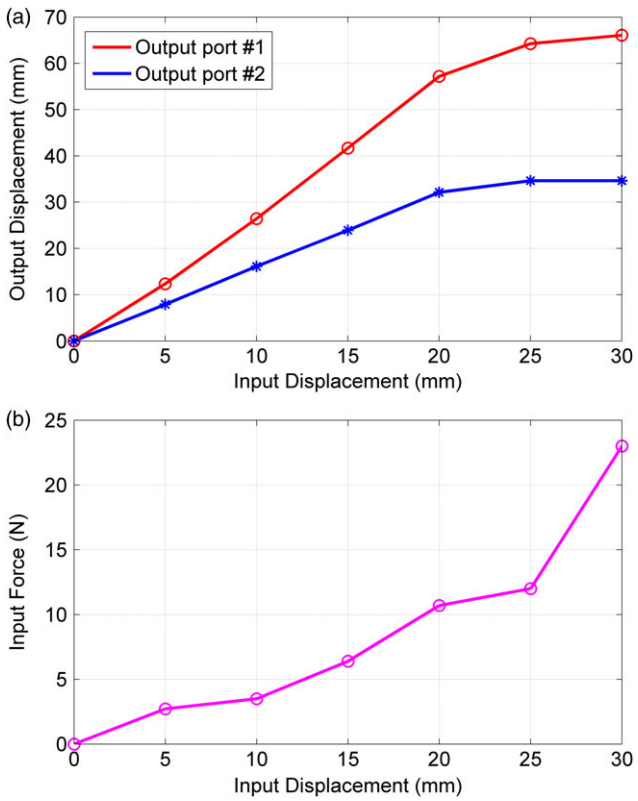

Fig. 11. Input–output relationships of the compliant gripper at free movement conditions: (a) input displacement versus output displacement, and (b) input displacement versus input force.

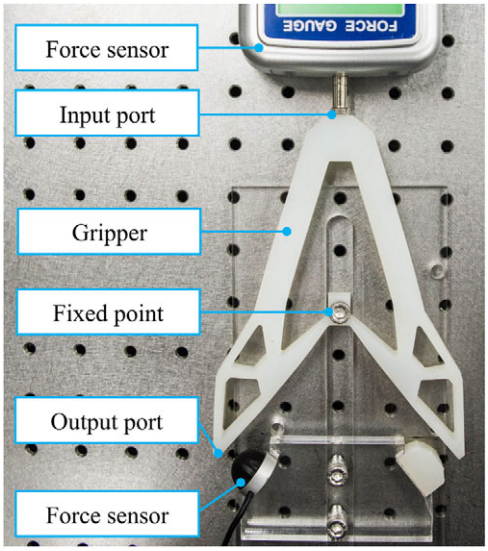

Fig. 12. Experimental setup for mechanical advantage test.

given in Table II with the experimental result (mechanical advantage = 0.28) as given in Fig. 13(b), the analysis result in the optimization stage has 95.4% accuracy.

Figure 14 shows the assembly of the robotic gripper, which consists of one linear actuator (HIWIN LAS1-2), two identical silicon rubber grippers, and aluminum frame. Figure 14(a) shows the side view of the gripper assembly, Fig. 14(b) shows the front view of the gripper assembly at open mode, and Fig. 14(c) shows the front view of the gripper assembly at closed mode. The linear actuator is used to generate input displacement for the gripper assembly. Two identical grippers are stacked together in order to increase the contact surfaces to improve grasping stability. Grip tests are

https://doi.org/10.1017/S0263574719000018 Published online by Cambridge University Press

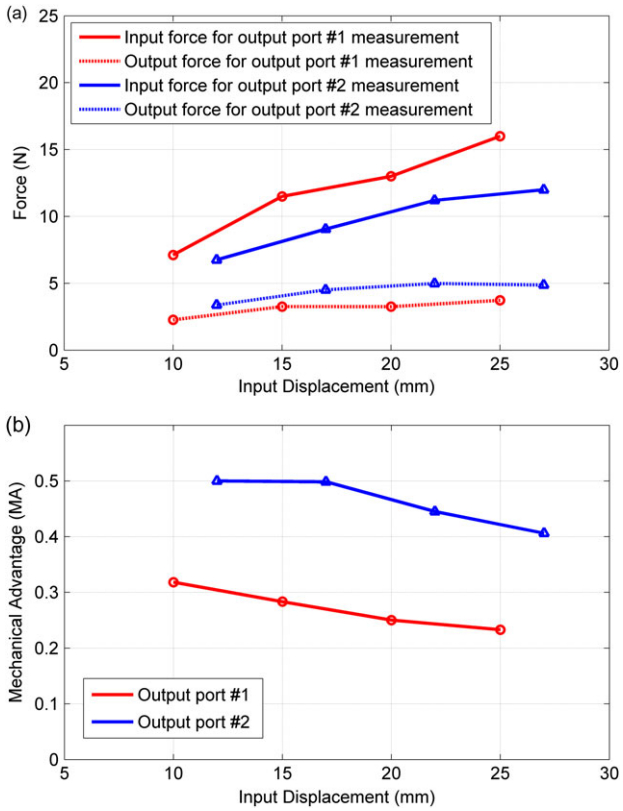

Fig. 13. Measurement results for one finger (a half gripper) from the mechanical advantage test: (a) force measurement results, and (b) mechanical advantage results.

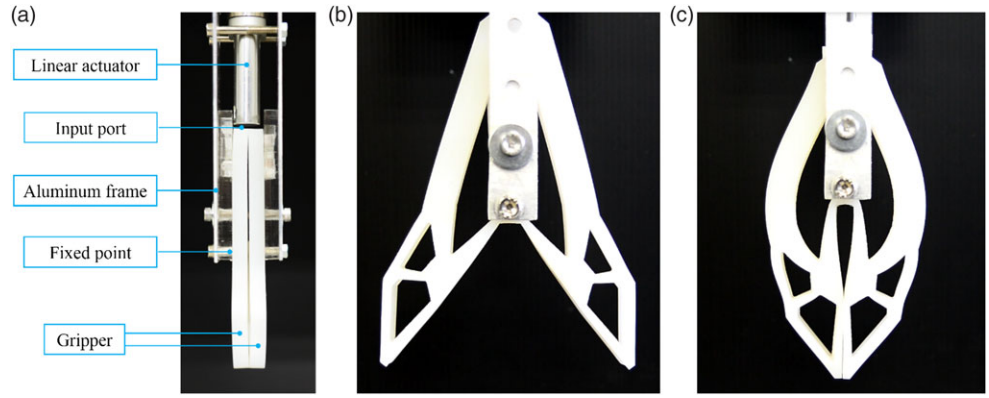

Fig. 14. Gripper assembly: (a) side view, (b) front view at open mode, and (c) front view at closed mode.

performed to demonstrate the design of the adaptive compliant gripper. Nine different objects (lemon, banana, power cable, plush toy, cucumber, book, helicopter toy, orange, and apple) handed by human are used in the grip test. The results are shown in Fig. 15. It is to be noticed that the proposed design can grip irregular objects with good adaptability (for both symmetric and nonsymmetric objects).

Payload tests for gripping both convex and concave objects as referred in Fig. 2 are performed to identify the adaptability and maximum allowable payload for the gripper assembly (as given in Fig. 14) at different operating conditions. The used convex and concave objects in the payload tests are shown in Fig. 16. The convex object is an aluminum cylinder with diameter of 40.3 mm and height of 50 mm. The concave object is a 3D-printed component with dimensions specified in Fig. 16; its thickness is 25 mm. To investigate the effect of friction of object surface on the maximum payload, an anti-slip foam tape is further applied on both objects to compare the identified maximum payload with and without anti-slip foam tape. The payload test results are given in Fig. 17. The experiments

https://doi.org/10.1017/S0263574719000018 Published online by Cambridge University Press

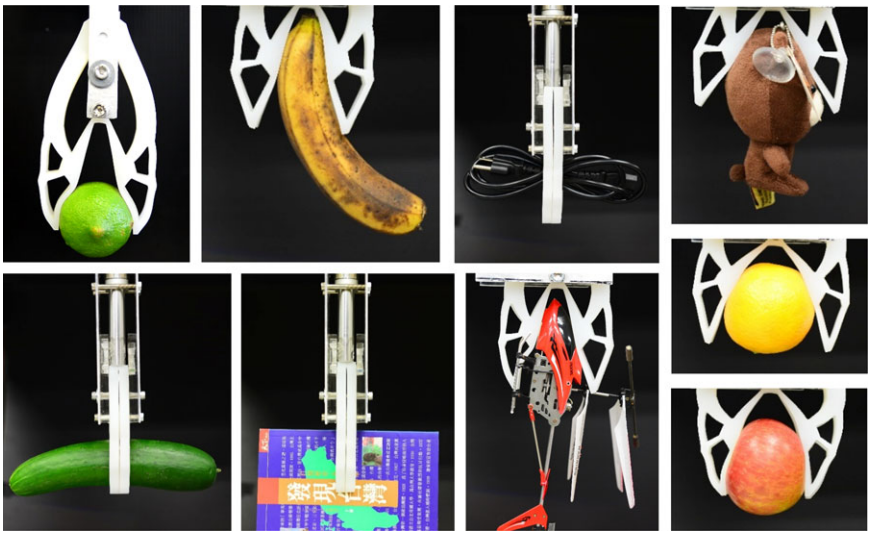

Fig. 15. Object grasping test (objects include lemon, banana, power cable, plush toy, cucumber, book, helicopter toy, orange, and apple).

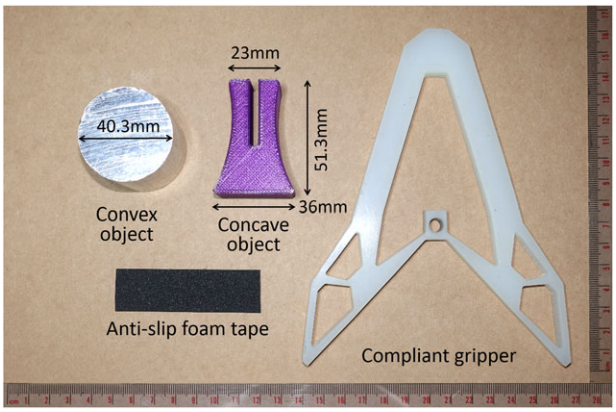

Fig. 16. Convex object, concave object, anti-slip foam tape, and gripper for the payload test.

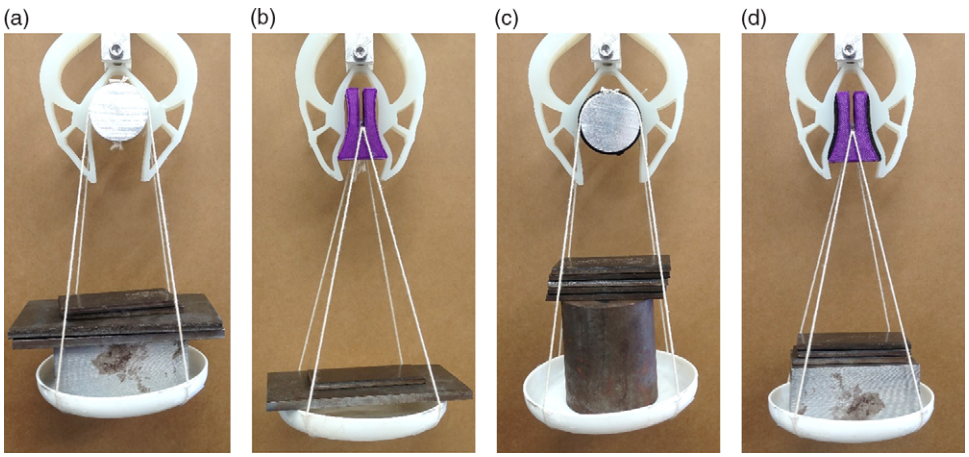

Fig. 17. Payload test: (a) convex object (max. payload = 2.5kg), (b) concave object (max. payload = 0.7kg), (c) convex object with anti-slip foam tape (max. payload = 2.7kg), and (d) concave object with anti-slip foam tape (max. payload = 1.4kg).

https://doi.org/10.1017/S0263574719000018 Published online by Cambridge University Press

are carried out iteratively by gradually increasing the number of mass blocks in the tray hanging on the gripped object. Figure 17(a) shows the payload test result for gripping the convex object without anti-slip foam tape; the maximum payload is identified as 2.5 kg for this condition. Figure 17(b) shows the payload test result for gripping the concave object without anti-slip foam tape; the maximum payload is identified as 0.7 kg for this condition. Figure 17(c) shows the payload test result for gripping the convex object with anti-slip foam tape; the maximum payload can increase from 2.5 to 2.7 kg compared with the condition without anti-slip foam tape. Figure 17(d) shows the payload test result for gripping the concave object with anti-slip foam tape; the maximum payload can increase from 0.7 to 1.4 kg compared with the condition without anti-slip foam tape. The test results show that the payload capacity varies according to the friction between gripper and object, as well as the geometry of the object. The best measured payload for the gripper assembly is 2.7 kg. In addition, the payload test results in Fig. 17 also show that the developed adaptive compliant gripper can grip both convex and concave objects with good adaptability as the grasping strategy illustrated in Fig. 2.

5. Conclusion

An optimal design procedure including topology optimization and size–shape optimization methods to maximize mechanical advantage of the synthesized compliant mechanism is presented. Topology optimization is used to synthesize the optimum layout of the compliant mechanism, whereas size–shape optimization is used to fine-tune the topology-optimized result. A new objective function for topology synthesis of compliant mechanisms with multiple output ports is proposed, which can take into account multiple output ports, mechanical advantage, and geometric advantage of the analyzed compliant mechanism through adjustable parameters. In order to increase the payload of the developed compliant gripper, the advantage control parameter used in this study is set to maximize mechanical advantage of the synthesized compliant mechanism, which is equivalent to maximizing the output force. The compliant gripper with higher mechanical advantage can grip heavier objects. The proposed methods are used to design an adaptive compliant gripper with high mechanical advantage. The topology-optimized result is used as the initial design domain for the size–shape optimization process, and an ALM-Simplex method is proposed to perform size–shape optimization of the topology-optimized result. The mechanical advantage of the topology-optimized gripper is increased by 9% after the size–shape optimization process. As the initial values of size–shape optimization are already topology-optimized, the variations of many geometric parameters are not significant after size–shape optimization. The proposed maximum mechanical advantage gripper is prototyped using silicon rubber. Experimental studies including mechanical advantage test, object grasping test, and payload test are carried out to evaluate the performance of the proposed design. The predicted mechanical advantage of the design in the optimization stage has 95.4% accuracy compared with the experimentally obtained result. The maximum payload of the proposed robotic gripper design is identified as 2.7 kg. The payload test results show that the load capacity of the gripper can vary according to the friction between gripper and object, as well as the geometry of the object. The gripping surface of the finger can be designed to be non-smooth to increase the surface friction, thereby increasing maximum payload. The developed two-finger, monolithic rubber gripper can grip objects through elastic deformation of its flexible structure. Further reliability analysis and tests should be carried out if excessive load or long-term operation conditions are applied on the design. The outcome of this study provides numerical methods to synthesize compliant mechanisms with higher output force, as well as to present an adaptive, monolithic compliant gripper for grasping irregular objects.

Acknowledgment

This work was supported by the grant, MOST 105-2221-E-006-082, from the Ministry of Science and Technology of Taiwan.

References

1. H. A. Eschenauer and N. Olhoff, "Topology optimization of continuum structures: A review," *ASME Appl. Mech. Rev.* **54**(4), 331–390 (2001).
2. G. I. N. Rozvany, "A critical review of established methods of structural topology optimization," *Struct. Multidiscipl. Optim.* **37**(3), 217–237 (2009).

https://doi.org/10.1017/S0263574719000018 Published online by Cambridge University Press

3. O. Sigmund and K. Maute, "Topology optimization approaches," *Struct. Multidiscipl. Optim.* **48**(6), 1031–1055 (2013).
4. N. P. van Dijk, K. Maute, M. Langelaar and F. van Keulen, "Level-set methods for structural topology optimization: A review," *Struct. Multidiscipl. Optim.* **48**(3), 437–472 (2013).
5. J. D. Deaton and R. V. Grandhi, "A survey of structural and multidisciplinary continuum topology optimization: Post 2000," *Struct. Multidiscipl. Optim.* **49**(1), 1–38 (2014).
6. M. P. Bendsøe, "Optimal shape design as a material distribution problem," *Struct. Multidiscipl. Optim.* **1**(4), 193–202 (1989).
7. M. P. Bendsøe and O. Sigmund, "Material interpolation schemes in topology optimization," *Arch. Appl. Mech.* **69**(9–10), 635–654 (1999).
8. M. P. Bendsøe and O. Sigmund, *Topology Optimization: Theory, Methods, and Applications* (Springer, Berlin, 2003).
9. A. Rietz, "Sufficiency of a finite exponent in SIMP (power law) methods," *Struct. Multidiscipl. Optim.* **21**(2), 159–163 (2001).
10. X. Huang and Y. M. Xie, "Convergent and mesh-independent solutions for the bidirectional evolutionary structural optimization method," *Finite Elem. Anal. Des.* **43**(14), 1039–1049 (2007).
11. X. Huang and Y. M. Xie, "Bi-directional evolutionary topology optimization of continuum structures with one or multiple materials," *Comput. Mech.* **43**(3), 393–401 (2009).
12. X. Huang and Y. M. Xie, *Evolutionary Topology Optimization of Continuum Structures: Methods and Applications* (Wiley, West Sussex, UK, 2010).
13. X. Huang, Y. Li, S. W. Zhou and Y. M. Xie, "Topology optimization of compliant mechanisms with desired structural stiffness," *Eng. Struct.* **79**, 13–21 (2014).
14. C. Alonso, O. M. Querin and R. Ansola, "A sequential element rejection and admission (SERA) method for compliant mechanisms design," *Struct. Multidiscipl. Optim.* **47**(6), 795–807 (2013).
15. C. Alonso, R. Ansola and O. M. Querin, "Topology synthesis of multi-material compliant mechanisms with a sequential element rejection and admission method," *Finite Elem. Anal. Des.* **85**, 11–19 (2014).
16. S. Rahmatalla and C. C. Swan, "Sparse monolithic compliant mechanisms using continuum structural topology optimization," *Int. J. Numer. Methods Eng.* **62**(12), 1579–1605 (2005).
17. H. Zhou, "Topology optimization of compliant mechanisms using hybrid discretization model," *ASME J. Mech. Des.* **132**(11), 111003 (2010).
18. H. Zhou and P. P. Killekar, "The modified quadrilateral discretization model for the topology optimization of compliant mechanisms," *ASME J. Mech. Des.* **133**(11), 111007 (2011).
19. B. Zhu, X. Zhang and S. Fatikow, "Level set-based topology optimization of hinge-free compliant mechanisms using a two-step elastic modeling method," *ASME J. Mech. Des.* **136**(3), 031007 (2014).
20. L. Cao, A. T. Dolovich and W. Zhang, "Hybrid compliant mechanism design using a mixed mesh of flexure hinge elements and beam elements through topology optimization," *ASME J. Mech. Des.* **137**(9), 092303 (2015).
21. C.-H. Liu and G.-F. Huang, "A topology optimization method with constant volume fraction during iterations for design of compliant mechanisms," *ASME J. Mech. Robot.* **8**(4), 044505 (2016).
22. C.-H. Liu, G.-F. Huang and T.-L. Chen, "An evolutionary soft-add topology optimization method for synthesis of compliant mechanisms with maximum output displacement," *ASME J. Mech. Robot.* **9**(5), 054502 (2017).
23. A. Krishnakumar and K. Suresh, "Hinge-free compliant mechanism design via the topological level-set," *ASME J. Mech. Des.* **137**, 031406 (2015).
24. D. Petković, N. D. Pavlović, S. Shamshirband and N. B. Anuar, "Development of a new type of passively adaptive compliant gripper," *Ind. Robot: Int. J.* **40**, 610–623 (2013).
25. O. Sigmund, "On the design of compliant mechanisms using topology optimization," *Mech. Struct. Mach.* **25**, 493–524 (1997).
26. S. Montambault and C. M. Gosselin, "Analysis of underactuated mechanical grippers," *ASME J. Mech. Des.* **123**, 367–374 (2001).
27. D. Rus and M. T. Tolley, "Design, fabrication and control of soft robots," *Nature* **521**, 467–475 (2015).
28. L. U. Odhner, L. P. Jentoft, M. R. Claffee, N. Corson, Y. Tenzer, R. R. Ma, M. Buehler, R. Kohout, R. D. Howe and A. M. Dollar, "A compliant, underactuated hand for robust manipulation," *Int. J. Robot. Res.* **33**(5), 736–752 (2014).
29. R. Deimel and O. Brock, "A novel type of compliant and underactuated robotic hand for dexterous grasping," *Int. J. Robot. Res.* **35**(1–3), 161–185 (2016).
30. X. Zhou, C. Majidi and O. M. O'Reilly, "Soft hands - An analysis of some gripping mechanisms in soft robot design," *Int. J. Solids Struct.* **64–65**, 155–165 (2015).
31. M. Manti, T. Hassan, G. Passetti, N. D'Elia, C. Laschi and M. Cianchetti, "A bioinspired soft robotic gripper for adaptable and effective grasping," *Soft Robot.* **2**(3), 107–116 (2015).
32. K. C. Galloway, K. P. Becker, B. Phillips, J. Kirby, S. Licht, D. Tchernov, R. J. Wood and D. F. Gruber, "Soft robotic grippers for biological sampling on deep reefs," *Soft Robot.* **3**(1), 23–33 (2016).
33. R. K. Katzschmann, A. D. Marchese and D. Rus, "Autonomous object manipulation using a soft planar grasping manipulator," *Soft Robot.* **2**(4), 155–164 (2015).
34. Y. Nishioka, M. Uesu, H. Tsuboi, S. Kawamura, W. Masuda, T. Yasuda and M. Yamano, "Development of a pneumatic soft actuator with pleated inflatable structures," *Adv. Robot.* **31**(14), 753–762 (2017).

https://doi.org/10.1017/S0263574719000018 Published online by Cambridge University Press

35. A. Pettersson, S. Davis, J. O. Gray, T. J. Dodd and T. Ohlsson, "Design of a magnetorheological robot gripper for handling of delicate food products with varying shapes," *J. Food Eng.* **98**, 332–338 (2010).
36. A. Pettersson, T. Ohlsson, S. Davis, J. O. Gray, and T. J. Dodd, "A hygienically designed force gripper for flexible handling of variable and easily damaged natural food products," *Innov. Food Sci. Emerg. Technol.* **12**, 344–351 (2011).
37. C.-H. Liu and K.-M. Lee, "Dynamic modeling of damping effects in highly damped compliant fingers for applications involving contacts," *ASME J. Dyn. Syst. Measur. Cont.* **134**, 011005 (2012).
38. K.-M. Lee and C.-H. Liu, "Explicit dynamic finite element analysis of an automated grasping process using highly damped compliant fingers," *Comput. Math. Appl.* **64**, 965–977 (2012).
39. M. Ceccarelli, G. Figliolini, E. Ottaviano, A. Mata and E. Criado, "Designing a robotic gripper for harvesting horticulture products," *Robotica* **18**(1), 105–111 (2000).
40. M. Russo, M. Ceccarelli, B. Corves, M. Hüsing, M. Lorenz, D. Cafolla and G. Carbone, "Design and test of a gripper prototype for horticulture products," *Robot. Comput.-Integ. Manuf.* **44**, 266–275 (2017).
41. F. Dimeas, D. Sako, V. Moulianitis and N. Aspragathos, "Design and fuzzy control of a robotic gripper for efficient strawberry harvesting," *Robotica* **33**(5), 1085–1098 (2015).
42. J. Ma, S.-L. Chen, C. S. Teo, C. J. Kong, A. Tay, W. Lin and A. A. Mamun, "A constrained linear quadratic optimization algorithm toward jerk-decoupling cartridge design," *J. Franklin Inst.* **354**(1), 479–500 (2017).
43. J. Ma, S.-L. Chen, N. Kamaldin, C. S. Teo, A. Tay, A. A. Mamun and K. K. Tan, "Integrated mechatronic design in the flexure-linked dual-drive gantry by constrained linear-quadratic optimization," *IEEE Trans. Ind. Elect.* **65**(3), 2408–2418 (2018).
44. S.-L. Chen, X. Li, C. S. Teo and K. K. Tan, "Composite jerk feedforward and disturbance observer for robust tracking of flexible systems," *Automatica*, **80**, 253–260 (2017).
45. O. Sigmund and J. Petersson, "Numerical instabilities in topology optimization: A survey on procedures dealing with checkerboards, mesh-dependencies and local minima," *Struct. Optim.* **16**(1), 68–75 (1998).
46. M. Zhou, Y. K. Shyy and H. L. Thomas, "Checkerboard and minimum member size control in topology optimization," *Struct. Multidiscipl. Optim.* **21**(2), 152–158 (2001).
47. T. A. Poulsen, "A simple scheme to prevent checkerboard patterns and one-node connected hinges in topology optimization," *Struct. Multidiscipl. Optim.* **24**, 396–399 (2002).
48. O. Sigmund, "Morphology-based black and white filters for topology optimization," *Struct. Multidiscipl. Optim.* **33**, 401–424 (2007).
49. S. S. Rao, *Engineering Optimization: Theory and Practice*, 4th edn. (John Wiley & Sons, Hoboken, New Jersey, 2009).

https://doi.org/10.1017/S0263574719000018 Published online by Cambridge University Press